Learning Controllable Adaptive Simulation for Multi-scale Physics

Tailin Wu[*]
Department of Computer Science
Stanford University
tailin@cs.stanford.edu

Takashi Maruyama[*]
NEC Corp. & Stanford University
49takashi@nec.com &
takashi279@cs.stanford.edu

Qingqing Zhao[*]
Department of Electrical Engineering
Stanford University
cyanzhao@stanford.edu

Gordon Wetzstein
Department of Electrical Engineering
Stanford University
gordon.wetzstein@stanford.edu

Jure Leskovec
Department of Computer Science
Stanford University
jure@cs.stanford.edu

Abstract

Simulating the time evolution of physical systems is pivotal in many scientific and engineering problems. An open challenge in simulating such systems is their multi-scale dynamics: a small fraction of the system is extremely dynamic, and requires very fine-grained resolution, while a majority of the system is changing slowly and can be modeled by coarser spatial scales. Typical learning-based surrogate models use a uniform spatial scale, which needs to resolve to the finest required scale and can waste a huge compute to achieve required accuracy. In this work, we introduce Learning controllable Adaptive simulation for Multi-scale Physics (LAMP) as the first full deep learning-based surrogate model that jointly learns the evolution model and optimizes appropriate spatial resolutions that devote more compute to the highly dynamic regions. LAMP consists of a Graph Neural Network (GNN) for learning the forward evolution, and a GNN-based actor-critic for learning the policy of spatial refinement and coarsening. We introduce learning techniques that optimizes LAMP with weighted sum of error and computational cost as objective, which allows LAMP to adapt to varying relative importance of error vs. computation tradeoff at inference time. We test our method in a 1D benchmark of nonlinear PDEs and a challenging 2D mesh-based simulation. We demonstrate that our LAMP outperforms state-of-the-art deep learning surrogate models with up to 39.3% error reduction, and is able to adaptively trade-off computation to improve long-term prediction error.

1 Introduction

Simulating the time evolution of a physical system is of vital importance in science and engineering (Lynch, 2008; Carpanese, 2021; Sircombe et al., 2006; Courant et al., 1967; Lelievre & Stoltz, 2016). Usually, the physical system has a multi-scale nature: a small fraction of the system is highly dynamic,

[*]Equal contribution

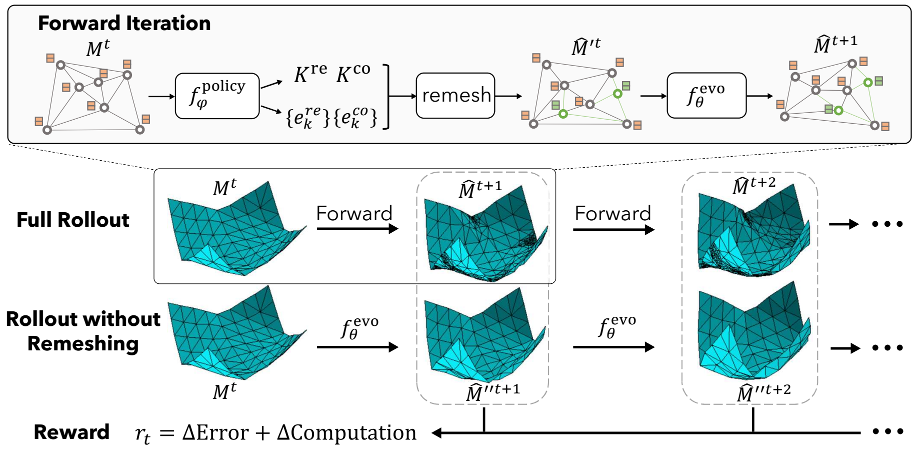

Figure 1: LAMP schematic. The forward iteration (upper box) first uses the policy $f_\varphi^{\text{policy}}$ to decide the number K^{re} and K^{co} of edges as well as which edges among the full mesh to be refined or coarsened, and then executes remeshing. The evolution model f_θ^{evo} is applied to the updated mesh $\hat{M}'^t$ to predict the state $\hat{M}^{t+1}$ at the next time step. We use the *reduction* of both *Error* and *Computation* (mesh size), compared to a multi-step rollout without remeshing, as reward to learn the policy.

and requires very fine-grained resolution to simulate accurately, while a majority of the system is changing slowly. Examples include hazard prediction in weather forecasting (Majumdar et al., 2021), disruptive instabilities in the plasma fluid in nuclear fusion (Kates-Harbeck et al., 2019), air dynamics near the boundary for jet engine design (Athanasopoulos et al., 2009), and more familiar examples such as wrinkles in a cloth (Pfaff et al., 2021) and fluid near the boundary for flow through the cylinder (Vlachas et al., 2022). Due to the typical huge size of such systems, it is pivotal that those systems are simulated not only *accurately*, but also with as small of a *computational cost* as possible. A uniform spatial resolution that pays similar attention to regions with vastly different dynamics, will waste significant compute on slow-changing regions while insufficient for highly dynamic regions.

To accelerate physical simulations, deep learning (DL)-based surrogate models have recently emerged as a promising alternative to complement (Um et al., 2020) or replace (Li et al., 2021) classical solvers. They reduce computation and accelerate the simulation with larger spatial (Um et al., 2020; Kochkov et al., 2021) or temporal resolution (Li et al., 2021), or via latent representations (Sanchez-Gonzalez et al., 2020; Wu et al., 2022). However, current deep learning-based surrogate models typically assume a uniform or fixed spatial resolution, without *learning* how to best assign computation to the most needed spatial region. Thus, they may be insufficient to address the aforementioned multi-scale challenge. Although adaptive methods, such as Adaptive Mesh Refinement (AMR) (Soner et al., 2003; Cerveny et al., 2019) exist for classical solvers, they share similar challenge (e.g. slow) as classical solvers. A deep learning-based surrogate models, that is able to learn both the evolution and learn to assign computation to the needed region, is needed.

In this work, we introduce Learning controllable Adaptive simulation for Multi-scale Physics (LAMP) as the first fully DL-based surrogate model that jointly learns the evolution model and optimizes appropriate spatial resolutions that devote more compute to the highly dynamic regions. Our key insight is that by explicitly setting the error and computation as the combined objective to optimize, the model can learn to adaptively decide the best local spatial resolution to evolve the system. To achieve this goal, LAMP consists of a Graph Neural Network (GNN)-based evolution model for learning the forward evolution, and a GNN-based actor-critic for learning the policy of discrete actions of local refinement and coarsening of the spatial mesh, conditioned on the local state and a coefficient β that weights the relative importance of error vs. computation. The policy (actor) outputs both the *number* of refinement and coarsening actions, and *which* edges to refine or coarsen, while the critic evaluates the expected reward of the current policy. The full system is trained with an alternating fashion, iterating between training the evolution model with supervised loss, and training the actor-critic via reinforcement learning (RL). Taken together, a single instance of evolution model and actor-critic jointly optimizes reduction of error and computation for the physical simulation, and can operate across the relative importance of the two metrics at inference time.

We evaluate our model on a 1D benchmark of nonlinear PDEs (which tests generalization across PDEs of the same family), and a challenging 2D mesh-based simulation of paper folding. In 1D, we show that our model outperforms state-of-the-art deep learning-based surrogate models in terms of long-term evolution error by up to 39.3%, and can adaptively tradeoff computation to improve long-term prediction error. On a 2D mesh-based simulation, our model can strategically choose appropriate edges to refine or coarsen, and outperforms a baseline without remeshing.

2 Problem Setting and Related Work

We consider the numerical simulation of a physical system, following the notation introduced in (Pfaff et al., 2021). The system's state at time t is discretized into the mesh-based state $M^t = (V^t, E^t), t = 0, 1, 2, ...$, where E^t is the mesh edges and V^t is the states at the nodes at time t. Each node $i \in V$ contains the mesh-space coordinate u_i and dynamic features q_i. Note that this representation of the physical system is very general. It includes Eulerian systems (Wu et al., 2022) where the mesh is fixed and the field q_i on the nodes are changing, and Lagrangian systems (Sanchez-Gonzalez et al., 2020; Pfaff et al., 2021) where the mesh coordinate in physical space is also dynamically moving (for this case, an additional world coordinate x_i is accompanying the mesh coordinate u_i). During prediction, a simulator f (classical or learned) autoregressively predicts system's state $\hat{M}^{t+1}$ at the next time step based on its previous prediction $\hat{M}^t$ at previous time step:

$$\hat{M}^{t+1} = f(\hat{M}^t), t = 0, 1, 2, ... \tag{1}$$

where $\hat{M}^0 = M^0$ is the initial state. During the prediction, both the dynamic features V^t at the mesh nodes, and the mesh topology E^t can be changing. The error is typically computed by comparing the prediction and ground-truth after long-term prediction: error $:= \ell(\hat{M}^t, M^t)$ for a metric ℓ (e.g. MSE, RMSE), and the computation cost (in terms of floating point operations, or FLOPs) typically scales with the size of the mesh (e.g. the number of nodes). The task is to evolve the system long-term into the future, with a low error and a constraint on the computational cost. We review related work in Appendix A.

3 Method

In this section, we detail our LAMP method. We first introduce its architecture in Sec. 3.1. Then we introduce its learning method (Sec. 3.2), including learning objective and training, and technique to let it learn to adapt to varying importance of error and computation.

3.1 Model architecture

The model architecture of LAMP consists of two components: an actor-critic which updates the mesh topology, and an evolution model which evolves the states defined on the mesh. We will detail them one by one.

Actor-critic. The actor-critic consists of a policy network $f_\varphi^{\text{policy}}$ (with parameter φ) which predicts the probability of performing the spatial coarsening or refining actions, and a value network f_φ^{value} which evaluates the long-term expected reward of the policy network:

$$P(A = a^t | M = M^t, \beta) = p_\varphi(a^t | M^t, \beta) = f_\varphi^{\text{policy}}(M^t, \beta) \tag{2}$$

$$\hat{v}^t = f_\varphi^{\text{value}}(M^t, \beta) \tag{3}$$

where a^t is the (refining and coarsening) action performed on the edges E^t so that it will become $\hat{E}^{t+1}$. The policy network $f_\varphi^{\text{policy}}$ outputs the probability of performing such action and can sample from this probability. v^t estimates the "value" of the current policy starting from current state M^t (for more information, see Sec. 3.2 below). The explicit dependence on β (as the β in Eq. 7) allows the policy and value network to condition on the varying importance of error and computation. Given the predicted mesh $\hat{E}^{t+1}$ and the current node features V^t on the current mesh E^t, an interpolation is performed which obtains the node features on the new mesh:

$$\hat{V}'^t = g^{\text{interp}}(V^t, \hat{E}^{t+1}, E^t) \tag{4}$$

Now the new intermediate state $\hat{M}'^t = (\hat{V}'^t, \hat{E}^{t+1})$ is defined on the new mesh $\hat{E}^{t+1}$.

Evolution model. The second component is an evolution model f_θ^{evo} which takes as input the intermediate state M'^t defined on $\hat{E}^{t+1}$, and outputs the prediction of node features $\hat{V}^{t+1}$ for time $t+1$:

$$\hat{V}^{t+1} = f_\theta^{\text{evo}}(M'^t) \tag{5}$$

Note that in this stage, the mesh topology $\hat{E}^{t+1}$ is kept constant, and the evolution model f_θ^{evo} (with parameter θ) learns to predict the state based on the current mesh.

Taken together, Eqs. (2)(4)(5) evolve the system state from M^t at time t to state $\hat{M}^{t+1} = (\hat{V}^{t+1}, \hat{E}^{t+1})$ at $t+1$. During inference, they are executed autoregressively following Eq. (1), to predict the system's future states $\hat{M}^t, t = 1, 2, 3, ...$, given an initial state M^0.

GNN architecture. One requirement for the evolution model f_θ^{evo}, policy network $f_\varphi^{\text{policy}}$ and value network f_φ^{value} is that they can operate on changing mesh topology E^t. Graph Neural Networks (GNNs) are an ideal choice that meets this requirement. Since we represent the system's state as mesh, we adopt MeshGraphNets (Pfaff et al., 2021) as the base architecture for the above three models. Specifically, we encode V^t as node features for the graph, and encode the mesh topology edges E^t and world edges as two types of edges, and the edge features depend on the relative positions in the mesh coordinates and world coordinates. Based on the graph, a processor network that consists of N layers of message passing is performed to locally exchange and aggregate the information:

$$Z_{ij}^{(e)n+1} = \text{MLP}_\theta^{(v)}(E_{ij}^n, Z_i^{(v)n}, Z_j^{(v)n}),\ Z_i^{(v)n+1} = \text{MLP}_\theta^{(v)}(Z_i^{(v)n}, \sum_j Z_{ij}^{(e)n+1}). \tag{6}$$

where $Z_i^{(v)n}$ is the latent node vector on node i at layer n, and $Z_{ij}^{(e)n}$ is the latent edge vectors on the n^{th} layer on the edge from node i to node j. We have $Z_i^{(v)0} = \hat{V}_i'^t$ and $Z_i^{(v)N} = \hat{V}_i^{t+1}$ are input and predicted node features at time t and $t+1$, respectively, in Eq. (5). Figure 1 provides an illustration of the architecture. We use an independent processor for the evolution model, and share the processor for the policy and value networks. After the processor, the latent vectors are concatenated with β to feed into downstream decoders. For the evolution model f_θ^{evo}, a decoder is operated on the latent state and outputs the prediction $\hat{V}'^{t+1}$ on the nodes. For the value network, an value MLP is operated on all nodes, and a global pooling is performed to compute the overall estimated value. For the policy network, we design the action decoder as follows.

Action representation. To predict the action for policy network and its probability, we first need to design the action space. Note that compared to typical reinforcement learning problems, here the action space is extremely high-dimensional and complicated: (1) each edge of the mesh may have the option of choosing refinement or coarsening. If there are thousands of edges N_{edge}, then the possible actions will be on the order of $2^{N_{\text{edge}}}$. (2) Not all actions are valid, and many combinations of actions are invalid. For example, two edges on the same face of the mesh cannot be refined at the same time, nor can they be both coarsened. To address this high-dimensionality action problem, we introduce the following design of action space, where for both refinement and coarsening, the policy network first samples integers $K^{\text{re}}, K^{\text{co}} \in \{0, 1, 2, ...K^{\max}\}$, and then independently samples K^{re} edges to perform refinement and K^{co} edges to perform coarsening, with proper filtering. The combined action is $a^t = (K^{\text{re}}, e_1^{\text{re}}, e_2^{\text{re}}, ...e_{K^{\text{refine}}}^{\text{re}}, K^{\text{co}}, e_1^{\text{co}}, e_2^{\text{co}}, ...e_{K^{\text{co}}}^{\text{co}})$, where $K^{\text{re}}, K^{\text{co}} \in \{0, 1, ...K^{\max}\}$, and $e_k^{\text{re}}, e_k^{\text{co}} \in E^t, k = 1, 2, ...$ The combined log-probability of choosing the action a^t is given by:

$$\log p_\varphi(a^t|M^t) = \log p_\varphi(K^{\text{re}}|M^t) + \sum_{k=1}^{K^{\text{re}}} \log p_\varphi(e_k^{\text{re}}|M^t) + \log p_\varphi(K^{\text{co}}|M^t) + \sum_{k=1}^{K^{\text{co}}} \log p_\varphi(e_k^{\text{co}}|M^t)$$

This action representation offers several benefits compared to independent sampling of action on each edge, detailed in Appendix B.

3.2 Learning

The ultimate goal of the learning for LAMP is to optimize the objective Eq. (7) as follows:

$$L = (1 - \beta) \cdot \text{Error} + \beta \cdot \text{Computation} \tag{7}$$

for a wide range of β. To achieve this, we break down the above objective into an alternative learning of two phases: learning the evolution model with objective L^{evo} that minimizes long-term evolution error, and learning the policy with objective L^{policy} that optimizes both the long-term evolution error and computational cost.

Learning evolution. In this phase, the evolution model f_θ^{evo} is optimized to reduce the multi-step evolution *error* for the evolution model. As before, we denote $M^{t+s}, t=0,1,2,...,s=0,1,...S$ as the state of the system at time $t+s$ simulated by the ground-truth solver with very fine-grained mesh, and denote $\hat{M}^{t+s}, t=0,1,2,...,s=0,1,2,..S$ as the prediction by the current LAMP following the current policy, up to a horizon of S steps into the future. We further denote $\hat{M}''^{t+s}, t=0,1,2,...,s=0,1,2,..S$ as the prediction by the current evolution model on the fine-grained mesh, where its mesh is provided as ground-truth mesh E^{t+s} at each time step. Then the loss is given by:

$$L^{\text{evo}} = L_S^{\text{evo}}[f_\varphi^{\text{policy}}, f_\theta^{\text{evo}}; \hat{M}^t] + L_S^{\text{evo}}[\mathbb{I}, f_\theta^{\text{evo}}; \hat{M}''^t] \tag{8}$$

$$= \sum_{s=1}^{S} \alpha_s^{\text{policy}} \ell(\hat{M}^{l+s}, M^{l+s}) + \sum_{s=1}^{S} \alpha_s^{\mathbb{I}} \ell(\hat{M}''^{l+s}, M^{l+s}) \tag{9}$$

Essentially, we optimize two parts of the evolution loss: (1) $L_s^{\text{evo}}[f_\varphi^{\text{policy}}, f_\theta^{\text{evo}}; \hat{M}^t]$ (first term) which is the evolution loss by following policy network $f_\varphi^{\text{policy}}$ and evolution model f_θ^{evo}, starting at initial state of $\hat{M}^t$ for S steps. (here α_s^{policy} is the coefficient for the s-step loss with loss function ℓ). This makes sure that evolution model f_θ^{evo} adapts to the current policy $f_\varphi^{\text{policy}}$ that designates proper computation. (2) The second part of the loss, $L_s^{\text{evo}}[\mathbb{I}, f_\theta^{\text{evo}}; \hat{M}''^t]$, is the evolution loss by using the ground-truth fine-grained mesh and evolved by the evolution model f_θ^{evo}, starting at initial state of fine-grained mesh $\hat{M}''^t$ and evolve for s steps. This encourages the evolution model to learn to utilize more computation to achieve a better prediction error.

Learning the policy. In this phase, the policy network $f_\varphi^{\text{policy}}$ learns to update the spatial resolution (refinement or coarsening of mesh) at each location, to improve both the *computation* and the prediction *error*. Since the spatial refinement and coarsening are both discrete actions, and the metric of computation is typically non-differentiable, we use Reinforcement Learning (RL) to learn the policy. Specifically, we model it as a Markov Decision Process (MDP), where the environment state is the system's state M^t, the actions are the local refinement or coarsening at each edge of E^t, and we design the reward as the *improvement* on both the error and computation, between following the current policy's action, and an *counterfactual* scenario where the agent follows an identity policy $\mathbb{I}$ that does not update the mesh topology, starting on the initial state $\hat{M}^t$. Concretely, the reward is:

$$r^t = (1-\beta)\cdot \Delta\text{Error} + \beta \cdot \Delta\text{Computation} \tag{10}$$

$$\Delta\text{Error} = L_S^{\text{evo}}[\mathbb{I}, f_\theta^{\text{evo}}; \hat{M}^t] - L_S^{\text{evo}}[f_\varphi^{\text{policy}}, f_\theta^{\text{evo}}; \hat{M}^t] \tag{11}$$

$$\Delta\text{Computation} = \mathcal{C}_S[\mathbb{I}, f_\theta^{\text{evo}}; \hat{M}^t] - \mathcal{C}_S[f_\varphi^{\text{policy}}, f_\theta^{\text{evo}}; \hat{M}^t] \tag{12}$$

Here $\mathcal{C}_S[\cdot]$ is a surrogate metric that quantifies the *computation* based on the predicted mesh topology $\hat{E}^{t+1}, \hat{E}^{t+2}, ...\hat{E}^{t+S}$ up to S steps into the future. In this paper we use the number of nodes as the surrogate metric for measuring the computation, since typically for the GNNs, the computation (in terms of FLOPs) scales linearly with the number of nodes (since each node has a bounded number of edges on the mesh, the number of edges thus also scales linearly with number of nodes, so will message passing and node updates).

To optimize the reward r^t, we employ the standard REINFORCE algorithm as used in (Sutton et al., 1999; Hafner et al., 2021) to update the policy network $f_\varphi^{\text{policy}}$, with the following objective:

$$L_\beta^{\text{actor}} = \mathbb{E}_t\left[-\log p_\varphi(a^t|M^t,\beta)\text{sg}(r^t - f_\varphi^{\text{value}}(M^t,\beta)) - \eta\cdot \text{H}[p_\varphi(a^t|M^t,\beta)]\right] \tag{13}$$

Here $\text{H}[\cdot]$ is the entropy, which encourages the action to have higher entropy to increase exploration, where η here is a hyperparameter. The $\text{sg}(\cdot)$ is stop-gradient. Essentially, the first term in loss L^{policy} encourages to increase the log-probability of actions that have a higher "advantage", where the advantage is defined as the difference between the current reward r^t that follows the current action a^t taken, and the expected reward (value) $f_\varphi^{\text{value}}(M^t,\beta)$ that follows the current policy starting from the current state M^t. We can also think of it as an actor-critic where the critic tries to evaluate accurately the expected reward of the current policy, and an actor (policy) is trying to exceed that expectation. To train the value network, we use MSE loss:

$$L_\beta^{\text{value}} = \mathbb{E}_t\left[(f_\varphi^{\text{value}}(M^t, \beta) - r^t)^2\right] \tag{14}$$

Learning to adapt to varying β. In the overall objective (Eq. 7), the β stipulates the relative importance between Error and Computation. $\beta = 0$ means we only focus on minimizing Error, without constraint on Computation. $\beta = 1$ means we only focus on minimizing computation, without considering the evolution error. In practice, we typically wish to improve both, with a $\beta \in (0, 1)$ that puts more emphasis on one metric but still considers the other metric. To allow LAMP to be able to operate at varying β at inference time, during the learning of policy, we sample β uniformly within a range $\mathcal{B} \subseteq [0, 1]$ (e.g. $\mathcal{B}$ can be $[0, 1]$ or $[0, 0.5]$), for different examples within a minibatch, and also train the policy and value network jointly, where the total loss L^{policy} is the weighted sum of the two policy and value losses:

$$L^{\text{policy}} = \mathbb{E}_{\beta\sim\mathcal{B}}[L_\beta^{\text{actor}} + \alpha^{\text{value}} \cdot L_\beta^{\text{value}}] \tag{15}$$

where α^{value} is a hyperparameter, which we set as 0.5. In this way, the policy can learn a generic way of spatial coarsening and refinement, conditioned on β. For example, for smaller β that focuses more on improving error, the policy network may learn to refine more on dynamic regions and coarsen less, sacrificing computation to improve prediction error.

4 Experiments

In the experiments, we set out to answer the following questions on our proposed LAMP: (1) Can LAMP learn to coarsen and refine the mesh, focusing more computation on the more dynamic regions to improve prediction accuracy? (2) Can LAMP improve the Pareto frontier of Error vs. Computation, compared to state-of-the-art deep learning surrogate models? (3) Can LAMP learn to condition on the β to change is behavior, and perform varying amount of refinement and coarsening depending on the β? We evaluate our LAMP on two challenging datasets: (1) a 1D benchmark nonlinear PDEs , which tests generalization of PDEs in the same family (Brandstetter et al., 2022); (2) a mesh-based paper simulation generated by the ArcSim solver (Narain et al., 2012). Both datasets possess multi-scale characteristics where some parts of the system is highly dynamic, while other parts are changing more slowly.

4.1 1D nonlinear family of PDEs

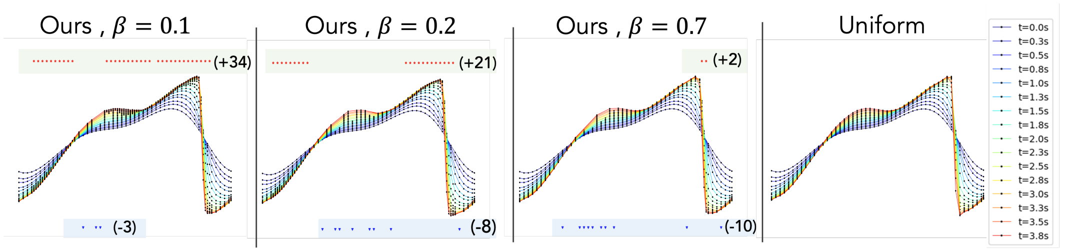

Figure 2: Example rollout result of our LAMP on 1D nonlinear PDEs with initial state on 50 vertices which is uniformly downsampled from the 100 vertices. The rollout is performed over 200 time steps, where different color denotes the system's state at different time. On each state, we also plot the corresponding mesh as black dots. The upper green and lower blue band shows the added and removed nodes of the mesh, comparing the end mesh and initial mesh. We see that with a smaller β (e.g. $\beta = 0.1$) that emphasizes more on "Error", it refines more on highly-dynamic regions (near shock front) and coarsens less. With a larger β (e.g. $\beta = 0.7$) that focuses more on reducing computation, it almost doesn't refine, and choose to coarsen on more static regions.

Data and Experiments. In this section, we test LAMP's ability to balance error vs. computation tested on unseen equations with different parameters in a given family. We use the 1D benchmark in Brandstetter et al. (2022), whose PDEs are given by

$$\left[\partial_t u + \partial_x(\alpha u^2 - \beta\partial_x u + \gamma\partial_{xx}u)\right](t,x) = \delta(t,x) \tag{16}$$

$$u(0,x) = \delta(0,x), \quad \delta(t,x) = \sum_{j=1}^{J} A_j \sin(\omega_j t + 2\pi\ell_j x/L + \phi_j) \tag{17}$$

The parameter for the PDE is given by $p = (\alpha, \beta, \gamma)$. The term δ is a forcing term (Bar-Sinai et al., 2019) with $J = 5, L = 16$ and coefficients A_j and ω_j sampled uniformly from $A_j \sim U[-0.5, 0.5]$, $\omega_j \sim U[-0.4, 0.4]$, $\ell_j \in \{1, 2, 3\}$, $\phi_j \sim U[0, 2\pi)$. We uniformly discretize the space to $n_x = 200$ in $[0, 16)$ and uniformly discretize time to $n_t = 250$ points in $[0, 4]$. Space and time are further downsampled to resolutions of $(n_t, n_x) \in \{(250, 100), (250, 50), (250, 33)\}$ as initial resolution. We use the **E2** scenario in the benchmark, which tests the model's ability to generalize to novel parameters of PDE with the same family. Specifically, we have that the parameter $p = (1, \eta, 0), \eta \sim U[0, 0.2]$.

As our LAMP autoregressively simulate the system, it can refine or coarsen the mesh at appropriate locations by the policy network $f_\varphi^{\text{policy}}$, before evolving to the next state with the evolution model f_θ^{evo}. We evaluate the models with the metric of Computation and long-term evolution Error. For the computation, we use the average number of vertices throughout the full trajectory as a surrogate metric, since the number of floating point operations typically scales linearly with the number of vertices in the mesh. For long-term evolution error, we use the cumulative MSE over rollout time steps, starting with initial state with a bundle of $S = 25$ time steps $t = [25, 26, ...49]$ and predict the rest 175 steps. We compare LAMP with strong baselines of deep learning-based surrogate models, including CNNs, Fourier Neural Operators (FNO) (Li et al., 2021), and MP-PDE (Brandstetter et al., 2022) which is a state-of-the-art deep learning-based surrogate models for this task. Our base neural architecture is based on MeshGraphNets (Pfaff et al., 2021) which is a state-of-the-art GNN-based model for mesh-based simulations. We compare an ablation of our model that does not perform remeshing (LAMP no remeshing), and a full version of our model (LAMP). We perform three groups of experiments, starting at initial number vertices of 33, 50 and 100 that is downsampled from the 100-vertex mesh, respectively. All the baselines do not perform remeshing, and our full model has the ability to perform remeshing that coarsen or refine the edges at each time step. Note that for all models, our metric of cumulative MSE is computed on the full ground-truth mesh with 100 vertices, where the values of prediction are linearly interpolated onto the location of the ground-truth. This prevents the model to "cheat" by reducing the number of vertices and only predict well on those vertices. Additional details are given in Appendix C.1.

Table 1: Result (error and computational cost) for 1D family of nonlinear PDEs, for a total rollout trajectory of 200 time steps, providing the first 25 steps as input.

Model	Initial # vertices	Average # vertices	Error (MSE)
CNN	33	33.0	2.66
FNO	33	33.0	2.83
MP-PDE	33	33.0	1.73
LAMP (no remeshing)	33	33.0	1.12
LAMP (ours)	33	37.6	**1.05**
CNN	50	50.0	1.10
FNO	50	50.0	1.79
MP-PDE	50	50.0	0.98
LAMP (no remeshing)	50	50.0	1.08
LAMP (ours)	50	53.2	**0.75**
CNN	100	100.0	0.81
FNO	100	100.0	1.39
MP-PDE	100	100.0	0.88
LAMP (no remeshing)	100	100.0	**0.75**
LAMP (ours)	100	100.0	0.76

Results. Table 1 shows the results. We see that our LAMP outperforms all baselines by a large margin, achieving an error reduction of 39.3%, 23.5% and 6.2% compared with the best performing baseline of CNN, FNO and MP-PDE. Importantly, we see that compared with an ablation with no remeshing, our full LAMP is able to significantly reduce error (by 6.3% error reduction for 33 initial vertices scenario, and 30.6% for 50 vertices scenario), with only slight increase of average number of vertices (by 13.9% and 6.4% increase, respectively). This shows the ability of LAMP to adaptively trade computation to improve long-term prediction error.

To investigate whether LAMP is able to focus computation on the most dynamic region, we visualize example trajectories of LAMP, as shown in Fig. 2 and more examples in Fig. 7 in Appendix D.1. Starting with 50 vertices, we test our model on different β, where smaller β focuses more on improving error. We see that with smaller β (e.g. $\beta = 0.1$ in Fig. 2), LAMP is able to add more nodes (33 nodes) on the most dynamic region, and only coarsen few (removing 3 nodes in total). With a larger β that focuses more on reducing computation, we see that LAMP refines less and coarsen more, and only coarsen on the more slowly changing region. Additionally, we visualize the error vs. number of vertices for varying β for two different models over all test trajectories in Fig. 3. We see that with increasing β, LAMP is able to reduce the vertices more, with only slight increase of error. In summary, the above results show that LAMP is able to focus computation on dynamic regions, and able to adapt to different β at inference.

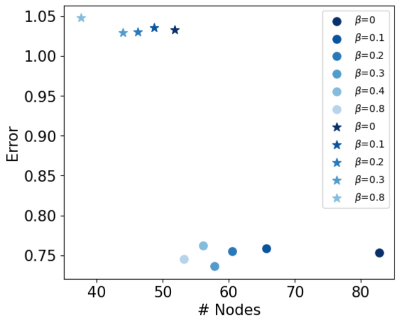

Figure 3: Error vs. average number of vertices with varying β, for two LAMP models trained with initial number of vertices of 33 (stars) and 50 (circles).

4.2 2D mesh-based simulation

Model	Initial # vertices	Average # vertices	Error (MSE)
LAMP (no remeshing)	81.0	81.0	1.9e-4
LAMP (ours)	81.0	87.9	1.6e-4

Table 2: Computation vs. Error for 2D mesh-based paper simulation between LAMP (with remeshing) and LAMP (without remeshing). With the proposed learned remeshing framework, LAMP are able to achieve better roll-out error with slight increase of average number of vertices. Reported number is the MSE over 10 learned-simulator-steps roll-out averaged over 50 test trajectories.

Here we evaluate our LAMP's ability on a more challenging setting with paper folding simulation. The paper in this simulation is square-shaped and its boundary edge length is 1. During the simulation, 4 corners of the paper receive different magnitude of force. When generating ground-truth trajectories by the ArcSim solver (Narain et al., 2012), we set the minimum and maximal length of edges to be 0.01 and 0.2. We evaluate the models with the metric of computation and long-term evolution error. Similar to the Section 4.1, we use the average number of nodes throughout the full trajectory as a surrogate metric for complexity. As shown in Table 2, our model is able to add more resolution to the high curvature region, and achieve better roll-out accuracy than the ablation without remeshing. Additional details (including visualization) of the experiments and 2D triangular mesh remeshing actions are given in Appendix C.2. In Fig. 6 in Appendix C.2 and Fig. 8 in Appendix D.2, we see that our LAMP learns to add more mesh onto the more dynamic regions near to the folding part (with high curvature), showing LAMP's ability to assign computation to the most needed region.

5 Conclusion

In this work, we have introduced LAMP, the first fully deep learning-based surrogate model that jointly learns the evolution of physical system and optimizes assigning the computation to the most dynamic regions. In 1D and 2D datasets, we show that our method is able to adaptively perform refinement or coarsening actions, which improves long-term prediction error than strong baselines of deep learning-based surrogate models. We hope our method provides a useful tool for more efficient and accurate simulation of physical systems.

References

Michael Athanasopoulos, Hassan Ugail, and Gabriela González Castro. Parametric design of aircraft geometry using partial differential equations. *Advances in Engineering Software*, 40(7):479–486, 2009.

Yohai Bar-Sinai, Stephan Hoyer, Jason Hickey, and Michael P Brenner. Learning data-driven discretizations for partial differential equations. *Proceedings of the National Academy of Sciences*, 116(31):15344–15349, 2019.

Johannes Brandstetter, Daniel E. Worrall, and Max Welling. Message passing neural PDE solvers. In *International Conference on Learning Representations*, 2022. URL `https://openreview.net/forum?id=vSix3HPYKSU`.

Francesco Carpanese. Development of free-boundary equilibrium and transport solvers for simulation and real-time interpretation of tokamak experiments. Technical report, EPFL, 2021.

Jakub Cerveny, Veselin Dobrev, and Tzanio Kolev. Nonconforming mesh refinement for high-order finite elements. *SIAM Journal on Scientific Computing*, 41(4):C367–C392, 2019.

Richard Courant, Kurt Friedrichs, and Hans Lewy. On the partial difference equations of mathematical physics. *IBM journal of Research and Development*, 11(2):215–234, 1967.

Stefan Elfwing, Eiji Uchibe, and Kenji Doya. Sigmoid-weighted linear units for neural network function approximation in reinforcement learning. *Neural Networks*, 107:3–11, 2018.

Christophe Geuzaine and Jean-François Remacle. Gmsh: A 3-d finite element mesh generator with built-in pre- and post-processing facilities. *International Journal for Numerical Methods in Engineering*, 79(11):1309–1331, 2009.

Danijar Hafner, Timothy P Lillicrap, Mohammad Norouzi, and Jimmy Ba. Mastering atari with discrete world models. In *International Conference on Learning Representations*, 2021. URL `https://openreview.net/forum?id=0oabwyZbOu`.

Xu Han, Han Gao, Tobias Pfaff, Jian-Xun Wang, and Liping Liu. Predicting physics in mesh-reduced space with temporal attention. In *International Conference on Learning Representations*, 2022. URL `https://openreview.net/forum?id=XctLdNfCmP`.

Julian Kates-Harbeck, Alexey Svyatkovskiy, and William Tang. Predicting disruptive instabilities in controlled fusion plasmas through deep learning. *Nature*, 568(7753):526–531, 2019.

Dmitrii Kochkov, Jamie A Smith, Ayya Alieva, Qing Wang, Michael P Brenner, and Stephan Hoyer. Machine learning–accelerated computational fluid dynamics. *Proceedings of the National Academy of Sciences*, 118(21), 2021.

Tony Lelievre and Gabriel Stoltz. Partial differential equations and stochastic methods in molecular dynamics. *Acta Numerica*, 25:681–880, 2016.

Zongyi Li, Nikola Borislavov Kovachki, Kamyar Azizzadenesheli, Burigede liu, Kaushik Bhattacharya, Andrew Stuart, and Anima Anandkumar. Fourier neural operator for parametric partial differential equations. In *International Conference on Learning Representations*, 2021. URL `https://openreview.net/forum?id=c8P9NQVtmnO`.

Peter Lynch. The origins of computer weather prediction and climate modeling. *Journal of computational physics*, 227(7):3431–3444, 2008.

Sharanya J Majumdar, Juanzhen Sun, Brian Golding, Paul Joe, Jimy Dudhia, Olivier Caumont, Krushna Chandra Gouda, Peter Steinle, Béatrice Vincendon, Jianjie Wang, et al. Multiscale forecasting of high-impact weather: current status and future challenges. *Bulletin of the American Meteorological Society*, 102(3):E635–E659, 2021.

Rahul Narain, Armin Samii, and James F O'brien. Adaptive anisotropic remeshing for cloth simulation. *ACM transactions on graphics (TOG)*, 31(6):1–10, 2012.

Tobias Pfaff, Meire Fortunato, Alvaro Sanchez-Gonzalez, and Peter W. Battaglia. Learning mesh-based simulation with graph networks. In *International Conference on Learning Representations*, 2021.

Alvaro Sanchez, Dmitrii Kochkov, Jamie Alexander Smith, Michael Brenner, Peter Battaglia, and Tobias Joachim Pfaff. Learning latent field dynamics of PDEs. *Advances in Neural Information Processing Systems*, 2020.

Alvaro Sanchez-Gonzalez, Jonathan Godwin, Tobias Pfaff, Rex Ying, Jure Leskovec, and Peter Battaglia. Learning to simulate complex physics with graph networks. In *International Conference on Machine Learning*, pp. 8459–8468. PMLR, 2020.

NJ Sircombe, TD Arber, and RO Dendy. Kinetic effects in laser-plasma coupling: Vlasov theory and computations. In *Journal de Physique IV (Proceedings)*, volume 133, pp. 277–281. EDP sciences, 2006.

Halil Mete Soner, Wolfgang Bangerth, Rolf Rannacher, Hans Foellmer, and LCG Rogers. *Adaptive finite element methods for differential equations*. Springer Science & Business Media, 2003.

Richard S Sutton, David McAllester, Satinder Singh, and Yishay Mansour. Policy gradient methods for reinforcement learning with function approximation. *Advances in neural information processing systems*, 12, 1999.

Kiwon Um, Robert Brand, Yun Raymond Fei, Philipp Holl, and Nils Thuerey. Solver-in-the-loop: Learning from differentiable physics to interact with iterative pde-solvers. *Advances in Neural Information Processing Systems*, 33:6111–6122, 2020.

Pantelis R Vlachas, Georgios Arampatzis, Caroline Uhler, and Petros Koumoutsakos. Multiscale simulations of complex systems by learning their effective dynamics. *Nature Machine Intelligence*, 4(4):359–366, 2022.

Tailin Wu, Takashi Maruyama, and Jure Leskovec. Learning to accelerate partial differential equations via latent global evolution. *Advances in neural information processing systems*, 36, 2022.

Qingqing Zhao, David B. Lindell, and Gordon Wetzstein. Learning to solve pde-constrained inverse problems with graph networks. *International Conference on Machine Learning*, 2022.

Appendix

A Related Works

Most classical solvers use a fixed mesh E^t whose topology does not vary with time. For example, the mesh $E^t \equiv E^0$ can be a 2D or 3D regular grid, or an irregular mesh that is pre-generated at the beginning of the simulation (Geuzaine & Remacle, 2009). Classical Adaptive Mesh Refinement (AMR) (Narain et al., 2012) addresses the multi-scale challenge by adaptively refine or coarsen the mesh resolution, with heuristics based on local state variation. Since they are based on classical solvers, they may not benefit from the many advantages that deep learning brings (GPU acceleration, less stringent spatial and temporal resolution requirement, explicit forward, etc.). In contrast, our LAMP is a deep-learning based surrogate model, and can benefit from the many advantages (e.g. speedup) offered by the deep learning framework. Furthermore, since it directly optimize for a linear combination of error and computation, it has the potential to directly optimize to a better error vs. computation tradeoff, nearer to the true Pareto frontier.

Deep-learning based surrogate models, although having achieved speedup compared to classical solvers, still typically operate on a fixed grid or mesh (Li et al., 2021; Sanchez et al., 2020; Wu et al., 2022; Zhao et al., 2022; Han et al., 2022), and have yet to exploit the multi-scale nature typical in physical simulations. One important exception is MeshGraphNets (Pfaff et al., 2021), which both learns how to evolve the state V^t, and uses supervised learning to learn the spatial adaptation that changes E^t. However, since it uses supervised learning where the ground-truth mesh is provided from the classical solver with AMR, it cannot exceed the performance of AMR in terms of error vs. computation tradeoff, and has to interact with the classical solver in inference time to perform the adaptive mesh refinement. In contrast, our LAMP directly optimizes for the objective, which uses reinforcement learning for learning the policy of refinement and coarsening, and has the potential to surpass classical AMR and achieve a better error vs. computation tradeoff. Moreover, a single trained LAMP has the ability to adapt to the full range of relative importance β of error vs. computation at inference time, thus can be more versatile than MeshGraphNets with a fixed strategy.

B Model Architecture

Here we detail the architecture of LAMP, complementary to Sec. 3.1. This architecture is used throughout all experiment, with just a few hyperparameter (e.g. latent dimension, message passing steps) depending on the dimension (1D, 2D) of the problem.

B.1 Architecture

In this subsection, we first detail the base architecture that is common among the evolution model f_θ^{evo}, the policy network $f_\varphi^{\text{policy}}$, and value network f_φ^{value}. Then describe their respective aspects, and explain the benefits of our action representation.

Base architecture. We use MeshGraphNets Pfaff et al. (2021) as our base architecture, for the evolution model f_θ^{evo}, the policy network $f_\varphi^{\text{policy}}$, and value network f_φ^{value}. All three models have an encoder and a processor. For the encoder, we encode both node features and edge features, uplift to latent dimension using MLPs, to Z_{ij}^e, Z_i^v. For the processor, it consists of N message passing layers. For each message-passing layer, we first update the edge features using current edge features, and connected node features, $Z_{ij}^{(e)n+1} = \text{MLP}_\theta^{(v)}(E_{ij}^n, Z_i^{(v)n}, Z_j^{(v)n})$, then we update the node features using current node feature and connected edge features, $Z_i^{(v)n+1} = \text{MLP}_\theta^{(v)}(Z_i^{(v)n}, \sum_j Z_{ij}^{(e)n+1})$. Depending on the models and their intended functions, different models have different modules for predicting the output, described as follows.

Evolution model. For the evolution model, the output is at each node, and uses the last latent vector on the node, feeds into a decoder, to predict the output $\hat{V}_i^{t+1} = Z_i^{(v)N}$ (See Eq. 6) at the next time step $t+1$.

Policy network and value network. Both $f_\varphi^{\text{policy}}$ and f_φ^{value} shares the same processor $f_\varphi^{\text{processor}}$, which has N message-passing layers. The final node feature is appended with β for the controllability.

The $f_{\varphi}^{\text{policy}}$ takes the encoded graph as input and consist of two parts - a global mean pooling is used to obtain the global latent representation of the whole graph, which is then fed into a MLP$^{(k)}$ followed by a action specific linear layer to predict the probability distribution for different number of actions should be performed; an action specific MLP$^{(a)}$ is applied on each edge to predict the probability of a certain action (i.e. split, coarse) to be applied on this edge. The $f_{\varphi}^{\text{value}}$ takes the same encoded graph as input, and perform a global mean pooling to obtain the global latent features for the graph, which is then feed through a linear layer to predict the accuracy reward, and another linear layer to predict the computation reward, the final predicted value is, $v = \text{loss} + \beta \cdot \text{compute}$.

Benefits of our action representation. Here we first elaborate the benefits of our action representation, compared to an independent sampling on each edge. If offers the following benefits:

- The action space reduces from $2^{N_{\text{edge}}}$ to ${N_{\text{edge}}}^{K^{\max}}$, where N_{edge} is the number of edges. In the case of $N_{\text{edge}} \sim 1000$ and $K^{\max} \sim 10 \ll N_{\text{edge}}$, the difference in action space dimensionality is significant, e.g. $2^{1000} = 10^{300}$ vs. $1000^{10} = 10^{30}$. Therefore, it is easier to credit assign the reward to appropriate action, with a smaller space of action.
- Compared with each edge performing action independently, now only $K \leq K^{\max}$ actions of refinement or coarsening can be performed. Therefore, it will need to focus on a few actions that can best improve the objective.
- The sampling of K will also make the policy more "controllable", since now the K is explicitly dependent on the β, and learning how many refinement or coarsening action to take depending on β is much easier than figuring out which concrete independent actions to take.

B.2 Architectural hyperparameters used in 1D and 2D experiments

Here we detail the architectures used in the 1D and 2D experiment. A summary of the hyperparameters is also provided in Table 3.

B.2.1 1D nonlinear PDEs

For 1D experiment, our evolution model f_{θ}^{evo} has $N = 3$ message-passing layers in the processor and latent dimension of 64. It uses the SiLU activation (Elfwing et al., 2018). The shared processor for $f_{\varphi}^{\text{policy}}$ and $f_{\varphi}^{\text{value}}$ has $N = 3$ message-passing layers and latent dimension of 64.

B.2.2 2D mesh-based simulation

For f_{θ}^{evo}, we set message passing layers for MeshGraphNets (Pfaff et al., 2021) to be 8. We also model our message passing function with MLP having 56 units followed by SiLU activation (Elfwing et al., 2018). Here, we share the same message passing function across all the 8 layers because we found in our experiments that sharing the same message passing function achieved better performance than having independent MLP for each of the layers. The shared processor for $f_{\varphi}^{\text{policy}}$ and $f_{\varphi}^{\text{value}}$ has $N = 3$ message-passing layers and latent dimension of 56.

C Experiment Details

In this section, we provide experiment details for 1D and 2D datasets. Firstly, we explain the use of reward r^t (in Eq. 13) as the value target instead of the typical recursive definition. Then we detail the training details for 1D and 2D in the following subsections.

Use of r^t as value target. Different from typical RL learning scenario (computer games or robotics) where the episode always has an end, and the reward is bounded, here in physical simulations, there are two distinct characteristics: (1) the rollout can be performed infinite time steps into the future, (2) as the rollout continues, at some point the error between predicted state and ground-truth state will diverge, so the error is not bounded. Based on these two characteristics, a value target based on the error for infinite horizon (e.g. the one used in Dreamer v2 (Hafner et al., 2021)) does not make sense, since it will not be bounded. In our experiment, we also observe similar phenomena, in which both the value target and value prediction continue to increase indefinitely. Thus, we use the average reward in the S step rollout as the value target, which measures the error and computation improvement within the rollout window we care about and proves to be much more stable.

C.1 1D nonlinear PDEs

The action space for 1D problem is composed with split and coarsen actions. The coarse action is initially defined on all edges, which is then sampled base on the predicted number of coarse actions, and probability of each edge to be coarsen. Among those sampled edges, if two edges share a common vertex, the right most one will be removed.

During training, to let the evolution model adapt to the varying size of the mesh, we perform random node dropout, where we randomly sample 10% of the minibatch to perform dropout, and if a minibatch is selected for node dropout, for each example, randomly drop 0-30% of the nodes in the mesh.

C.2 2D mesh-based simulation

In this subsection, we give details on remeshing actions and how to generate 2d mesh data based on Narain et al. (2012). We also details pre-training of our evolution function.

Action Space. There are 3 kinds of actions defined in the 2D mesh simulation: split, flip, and coarsen. Split action in 2D case can be performed on any edges that are shared with two triangular faces in a mesh and also on the boundary edges of the mesh. The split action results in 4 triangles (Fig. 4a). Flip action is also performed on edges shared with two faces, but it also requires some additional condition, that is when sum of angles at vertices located at opposite side of edges is greater than π: see also Fig 4b. In our remeshing function, all edges satisfying the condition are flipped. Finally, coarsen action has relatively strong conditions. One condition is that one of the source or target nodes of a coarsened edge needs to be of degree 4 and another condition is that all the faces connected to the node of degree 4 needs to have acute angles except angles around the node. See also Fig. 4c. We filter the sampled actions from $f_\varphi^{\text{policy}}$ base on aforementioned conditions to get sets of valid edges to split and coarse.

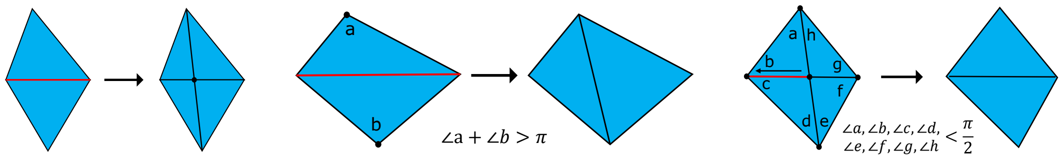
a
b
$\angle a + \angle b > \pi$
a
h
b
g
c
f
d
e
$\angle a, \angle b, \angle c, \angle d, \angle e, \angle f, \angle g, \angle h < \frac{\pi}{2}$

(a) Split action. (b) Flip action. (c) Coarsen action.

Figure 4: Illustration of split, flip and coarsen actions. The actions are performed on edges.

Generating data. To generate ground-truth data, we use a 2D triangular mesh-based AMR simulator Narain et al. (2012). This simulator adopts adaptive anisotropic kernel method to automatically conform to the geometric and dynamic detail of the simulated cloth: see also Fig. 5. In our experiment, each trajectory consists of 325 meshes (excluding initial mesh.) Each mesh consists of vertices and faces and every vertex is equipped with its 2D coordinates as well as 3D world coordinates. Time frame between two consecutive meshes are set to be 0.04. The edge length was set to range between 0.01 and 0.2. Note that decision on respective remeshing actions is made based on the 2D coordinates.

For training and test dataset, we generate 1050 configurations specifying direction and magnitude of forces applied to 4 corners of meshes, and generate 1000 trajectories for training data and use 50 trajectories as test data based on the generated configurations. When training our evolution model, we downsample data by half of the original data; we use every other meshes starting from an initial mesh in each trajectory. The reason of downsampling is that we observed that cumulative RMSE over rollout with model trained with full trajectories blew up after iteration exceeded 160 steps.

Pre-training of Evolution function. We model our evolution function f_θ^{evo} with MeshGraphNets (Pfaff et al., 2021). The input of the model adopts a graph representation where a vertex is equipped with 3D velocity computed from mesh information at both current and past time steps, and feature for an edge consists of relative distance and its magnitude of boundary vertices of the edge. Since

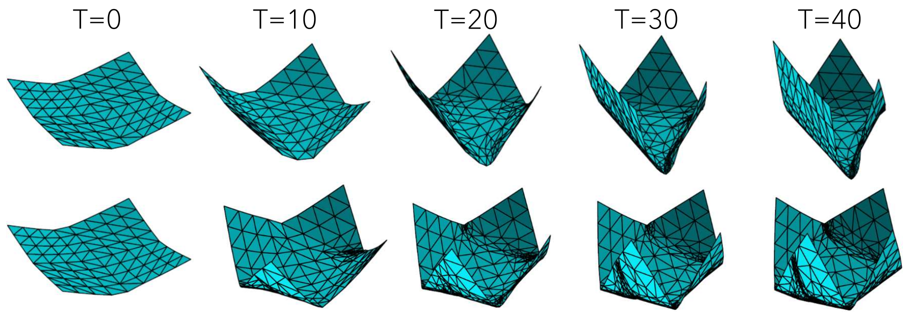

Figure 5: Part of trajectories generated with different configurations. As the time goes, finer triangular faces are added to high-curvature regions in meshes.

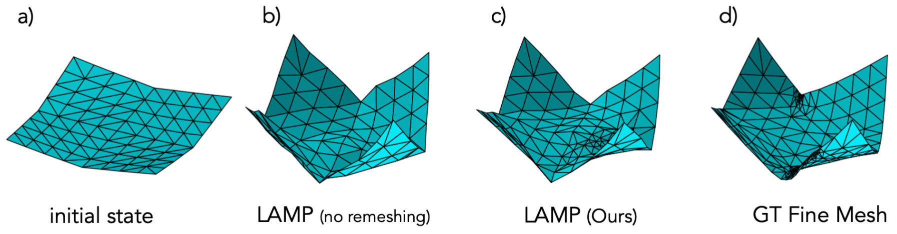

Figure 6: Example result of 2D mesh-based paper simulation. We observed that LAMP is adding more resolution to the high-curvature region to resolve the details. Figure a) is at $t = 0$, and figure b), c) and d) are LAMP (no remeshing), LAMP (ours) and ground truth results at $t = 30$.

mesh topology varies during the forward iteration, we perform barycentric interpolation on the mesh at past time step to get interpolated vertex coordinates corresponding to vertices at current time step.

When evaluating our model, we use rollout RMSE, taking the mean for all spatial coordinates, all mesh nodes, all steps in each trajectory, and all 50 trajectories in the test dataset. The rollout RMSE achieved 4.45×10^{-2} with our best parameter setting. We found that adding noise helped to improve its performance; we added the noise with scale 0.01 to vertex coordinates.

D Additional visualization

D.1 1D nonlinear PDE experiment

In this section, we provide additional randomly sampled results for the 1D nonlinear PDE experiment, as shown in Fig. 7. We see that similar to Fig. 2, our LAMP is able to add more vertices to the locations with more dynamicity, while remove more vertices at more static regions. Moreover, with increasing β that emphasizes more on reducing computational cost, LAMP splits less and coarsens more.

D.2 Additional visualization for 2D mesh-based simulation

In this section, we provide additional randomly sampled results for the 2D mesh-based simulation.

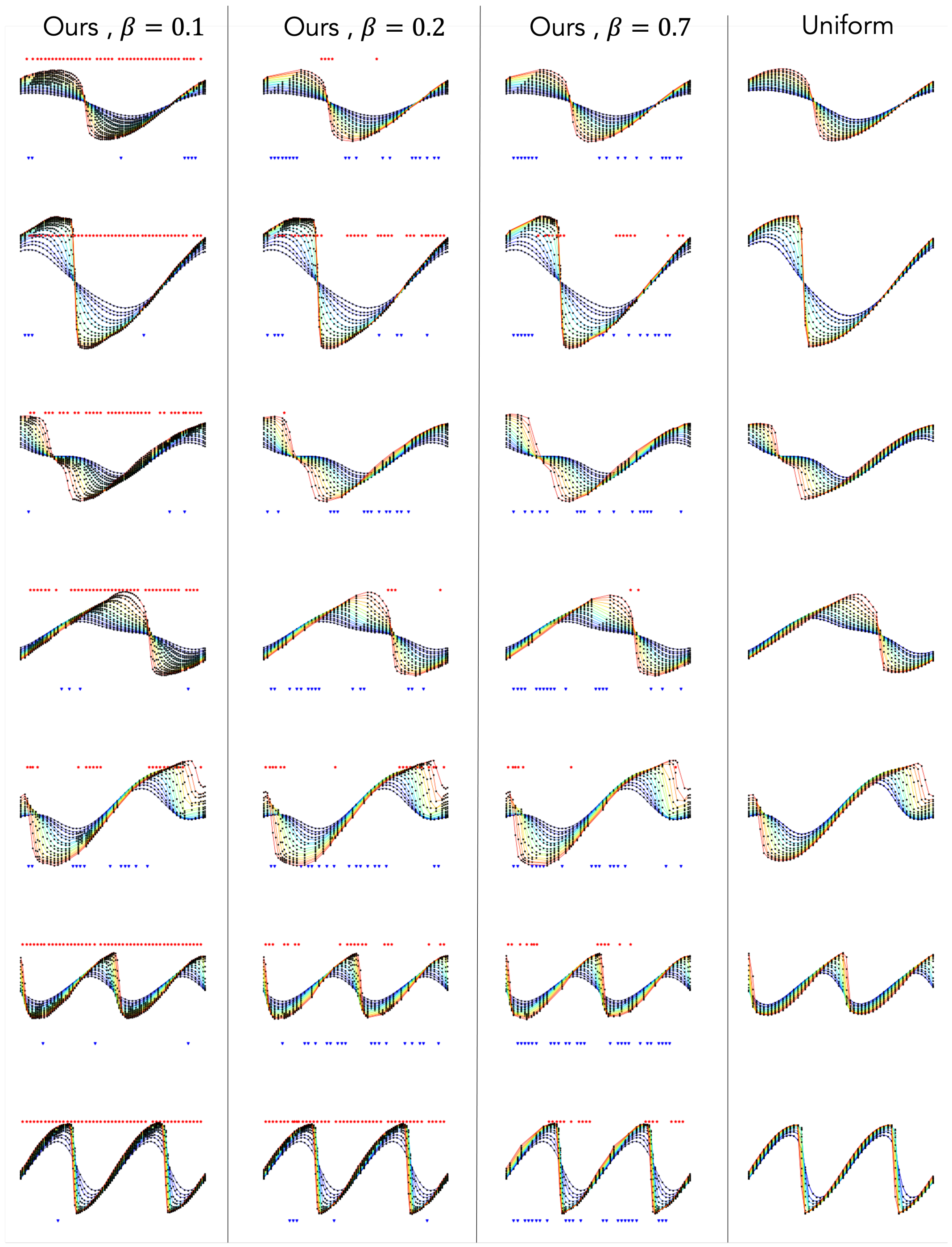

Figure 7: Additional example rollout results with different β of our LAMP on 1D nonlinear PDEs with initial state on 50 vertices which is uniformly downsampled from the 100 vertices. The rollout is performed over 200 time steps, where different color denotes the system's state at different time. The upper red dots and lower blue dots shows the added and removed nodes of the mesh, comparing the end and the initial mesh.

Table 3: Hyperparameters used for training the evolution model and actor-critic.

Hyperparameter name	1D dataset	2D dataset
Hyperparameters for model architecture:		
Temporal bundling steps	25	1
f_θ^{evo}: Latent size	64	56
f_θ^{evo}: Activation function	SiLU	SiLU
f_θ^{evo}: Encoder MLP number of layers	3	4
f_θ^{evo}: Processor number of message-passing layers	3	8
$f_\varphi^{\text{policy}}$: Latent size	64	56
$f_\varphi^{\text{policy}}$: Activation function	ELU	ELU
$f_\varphi^{\text{policy}}$: Encoder MLP number of layers	2	2
$f_\varphi^{\text{policy}}$: Processor number of message-passing layers	3	3
$f_\varphi^{\text{policy}}$: MLP$^{(k)}$: MLP number of layers	2	2
$f_\varphi^{\text{policy}}$: MLP$^{(k)}$: Activation function	ELU	ELU
$f_\varphi^{\text{policy}}$: MLP$^{(a)}$: MLP number of layers	3	3
$f_\varphi^{\text{policy}}$: MLP$^{(a)}$: Activation function	ELU	ELU
Hyperparameters for training:		
β sampling range $\mathcal{B}$	$[0, 0.5]$	$[0, 0.5]$
Loss function	MSE	L2
Number of epochs for pre-training evolution model	50	100
Number of epochs for training actor-critic	30	30
Batch size	128	16
Evolution model learning rate for pre-training	10^{-3}	10^{-3}
Evolution model learning rate during policy learning	10^{-4}	10^{-4}
Value network learning rate	10^{-4}	10^{-4}
Policy network learning rate	5×10^{-4}	5×10^{-4}
Optimizer	Adam	Adam
Coefficient for value loss	0.5	0.5
Maximum number of actions $K^{\max}$	20	20
Maximum gradient norm	2	2
Optimizer scheduler	cos	cos
Input noise amplitude	0	10^{-2}
Horizon S	4	4
Weight decay	0	0
Entropy coefficient η	10^{-2}	2×10^{-3}

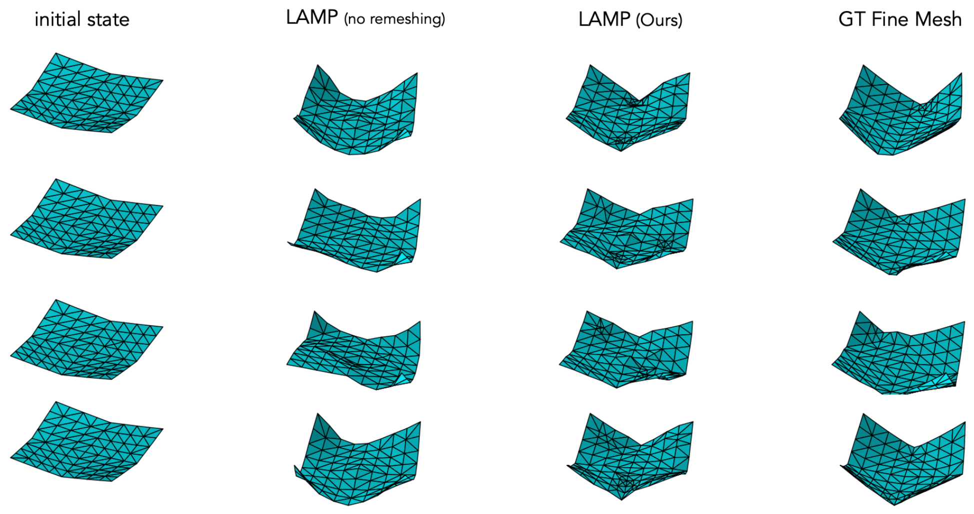

Figure 8: Additional example rollout results for 2D paper folding, at $t = 15$. We see that our LAMP (third column) learns to add more edges to locations with higher curvature, resulting in better rollout performance than with no remeshing.